PostScript file created: July 14, 2005

Relation between mainshock rupture process and Omori's law for aftershock moment release rate

Yan Y. Kagan[1] and Heidi Houston[1]

[1] Department of Earth and Space Sciences, University of California, Los Angeles, California, USA

Abstract. We compare the source time functions (moment release rates) of three large California mainshocks with the seismic moment release rates during their aftershock sequences. Aftershock moment release rates, computed by summing aftershock moments in time intervals, follow Omori's law from minutes to months after the mainshock; furthermore, in contrast to the previously-observed saturation in numbers of aftershocks shortly after the mainshock rupture, no such saturation is seen in the aftershock moment release rates, which are dominated by the largest aftershocks. We argue that the observed saturation in aftershock numbers described by the "time offset" parameter c in Omori's law is likely an artifact due to the under-reporting of small aftershocks, which is related to the difficulty of detecting large numbers of small aftershocks in the mainshock coda. We further propose that it is more natural for c to be negative (i.e., singularity follows the onset of mainshock rupture) than positive (singularity precedes onset of rupture). To make a more general comparison of mainshock rupture process and aftershock moment rates, we then scale mainshock time functions to equalize the effects of the varied seismic moments. For the three California mainshocks, we compare the scaled time functions with similarly-scaled aftershock moment rates. Finally, we compare global averages of scaled time functions of many shallow events to the average scaled aftershock moment release rate for six California mainshocks. In each of these comparisons, the extrapolation of the aftershock moment rates according to Omori's law back in time toward the mainshock rupture indicates that the temporal intensity of the aftershock moment release is about 1.5 orders of magnitude less than the maximum reached by the mainshock rupture. This may be due to the differing amplitudes and relative importance of static and dynamic stresses in aftershock initiation compared to mainshock rupture propagation.

Index terms: Seismology (ESE): 7215 Earthquake parameters; 7209 Earthquake dynamics and mechanics;

Keywords: Mainshock source-time functions; Seismic moment release; Omori's law; Static and dynamic stress triggering

1. Introduction

In this work we compare source-time functions (seismic moment release rates) for California and global shallow large earthquakes with the seismic moment release rate of aftershock sequences. By using moment release rate rather than the number of aftershocks we circumvent the problem of missing weak aftershocks, since most of the total moment in earthquake sequences is contained in the largest events (Kagan, 2002). Because we are interested in the transition between the mainshock rupture process and the beginning of the aftershock sequence, we need to use data from regional and local earthquake catalogs, based on interpretation of high frequency seismograms, rather than global catalogs as the former record aftershocks which are closer in time to the mainshock rupture end than global catalogs (Kagan, 2004).

We use available source-time histories for several large California earthquakes to infer the relation between mainshock rupture process and moment release in their immediate aftershocks. We also analyze source-time functions for global shallow earthquakes. Aftershock sequences of large earthquakes in southern California (1952 Kern County, 1992 Joshua Tree–Landers–Big Bear sequence, 1994 Northridge, and 1999 Hector Mine), recorded in the CalTech catalog are analyzed to demonstrate that from minutes to months after the mainshock the moment release follows Omori's law.

0148-0227/05/$9.00

2. Temporal distribution of aftershocks

Omori (1894, Eq. (b) p. 117) found that aftershock rate for the 1891 Nobi and two other Japanese earthquakes decayed about as

$$n(t) = \frac{K}{t+c}\,, \tag{1}$$

where K and c are coefficients, t is the time since mainshock origin, and $n(t)$ is the aftershock frequency measured over a certain interval of time. Presently a more complicated equation is commonly used to approximate aftershock rate

$$n(t) = \frac{K}{(t+c)^p}\,. \tag{2}$$

This expression with the additional exponent parameter p is called the modified Omori formula (Utsu, 1961; Utsu *et al.*, 1995). Here we assume that the exponent p is 1.0, its typical value in empirical studies.

The aftershock rate decay still continues now in the focal zone of the 1891 Nobi earthquake (Utsu *et al.*, 1995).

Statistical analysis of earthquake catalogs indicates that a power-law dependence characterizes the occurrence of both foreshocks and aftershocks. From this point of view a mainshock may be considered as an aftershock which happens to be stronger than the previous event (Kagan & Knopoff, 1981; Agnew, 2005; Gerstenberger *et al.*, 2005).

The parameter c in (1) is almost always found to be positive and typically ranges from 0.5 to 20 hours in empirical studies (Reasenberg & Jones, 1989; 1994; Utsu, 1961; Utsu *et al.*, 1995). It was introduced to explain the seeming saturation of aftershock rate close to the origin time of a mainshock. No reliable empirical regularities in the behavior of c have been found. Positive c in (1) means that the singularity in (1) occurs *before* the mainshock, which is unphysical. Negative c means that the singularity occurs after the mainshock. The latter case is a more physically natural assumption. In this case, $n(t)$ is not defined for the period $t \leq -c$. This could correspond, for example, to the period of mainshock rupture, during which individual aftershocks cannot be defined, identified, or counted. However, Eq. 1 assumes that earthquakes are instantaneous, therefore, for times comparable to the rupture time of mainshocks Omori's law breaks down, since earthquake counting is not possible for such small time intervals. Moreover, Omori's law in its regular form (1) and (2) predicts that for time $t \to 0$ the aftershock rate stabilizes around K/c. Again, aftershock counting is not feasible at the time of mainshock rupture and its coda, hence some time limit (Ogata, 1983) needs to be introduced in (1) and (2).

Fig. 1 shows Omori's law curves in the linear scale, whereas in Fig. 2 we display the curves in the more common log-log format. In the log-log case the line with a positive value of c describes a saturation of aftershock rate close to the earthquake origin time. Such a 'saturation' has been observed in many aftershock sequences (Reasenberg & Jones, 1989; 1994; Utsu *et al.*, 1995; for more discussion and references see Kagan, 2004). The saturation is usually interpreted as a delay between mainshock rupture end and the start of aftershock activity (Rundle *et al.* 2003; Kanamori & Brodsky, 2004).

Kagan (2004) argues that the real cause of this apparent rate saturation is not a physical property of aftershock sequences, but is due to under-reporting of short-term aftershocks, especially smaller ones in earthquake catalogs. Peng & Vidale (2004) and Vidale *et al.* (2003; 2004) note that the number of aftershocks in the first few minutes of the sequence observed on high-pass filtered seismograms is several times higher than aftershock numbers recorded in local catalogs. Shcherbakov *et al.* (2004) find that the parameter c in Omori's law decreases as the magnitude of earthquakes considered increases. They attribute this dependence to "the undercounting of small aftershocks at short times." Chen *et al.* (2004; 2005) find that in the 1999 Chi-Chi, Taiwan earthquake, aftershocks start after passing of rupture front and they decay according Omori's law even when rupture continues at more distant parts of earthquake fault. These results support our interpretation.

3. Seismic moment release in earthquakes and aftershocks

3.1. Three California earthquakes and their aftershocks

Fig. 3 displays seismic moment release curves (i.e., source time functions) for three recent large California earthquakes. These functions for the Landers, Northridge, and Hector Mine mainshocks have been obtained by Dreger (1994), by Thio & Kanamori (1996), and Ji *et al.* (2002), respectively. The apparent duration of earthquake rupture increases with earthquake size.

In Fig. 4 we show the aftershock distribution for the 1992 Northridge, California earthquake. The general time-magnitude aftershock pattern is seen in many other aftershock sequences (Kagan, 2004): larger aftershocks begin early in the sequence, whereas the occurrence rate is progressively delayed for weaker events. Above the threshold, aftershocks in any magnitude band seem to be distributed almost uniformly over log time, which would correspond to their rate decay according to Omori's law (1). As Kagan (2004) argues (see also Wiemer & Katsumata, 1999, their Fig. 2 and Wiemer *et al.*, 2002, their Fig. 2) the magnitude threshold in early aftershock sequences decreases with time. Therefore, the aftershock magnitude threshold approximation by (6) (see below) is also shown.

Fig. 5 shows moment release rates during the 1994 Northridge, California earthquake and during its aftershock sequence. We subdivide time after the mainshock origin into intervals increasing by a factor of 2, and sum the scalar seismic moments of its recorded aftershocks (Kagan, 2004). For most of the aftershocks seismic moment was not determined. We assume that their local magnitude is equivalent to the moment magnitude m (Hutton & Jones, 1993) and calculate the moment M (in Nm) as

$$M = 10^{1.5(m+6)}, \tag{3}$$

(Hanks, 1992).

Fig. 5 suggests that the aftershock moment rate $\dot{M}(t)$ can be approximated by by a power-law time dependence similar to Omori's law

$$\dot{M}(t) \;=\; \frac{k\,\tau_{pk}\,\dot{M}_{pk}}{t+c}\,, \tag{4}$$

where t is time after mainshock origin, c is a coefficient similar to that in (1), but possibly different in value, $\dot{M}_{pk}$ is the peak moment release rate of a mainshock and τ_{pk} is the time the peak occurs. The coefficient k characterizes the ratio of peak mainshock moment rate ($\dot{M}_{pk}$) and aftershock moment rate extrapolated to τ_{pk} (with $c = 0$). We do not yet know how close the end of mainshock moment release comes to the beginning of the aftershock process; it is possible that there is no actual temporal gap between these two phenomena (Kagan, 2004).

As Kagan (2004) notes, during the occurrence of a mainshock the rupture process is often punctuated by significant changes in moment rate amplitude, momentarily stopping or restarting rupture and other rupture complexities. As a result, large earthquakes in a detailed analysis are often subdivided into several sub-events. Aftershock moment release, on the other hand, is calculated by summing the moments of several separate events. It seems possible that in the transition time interval after mainshock rupture end and the beginning of the recorded aftershock sequence, the moment release could exhibit intermediate features – quasi-continuous rupture episodes which are supplanted by more discrete events. In part our recognition of distinct events is effected by the limited frequency content of seismograms, the presence of noise, etc. With ideal recording, the difference between mainshock and aftershock moment release rates may not be clear, abrupt, or well-defined.

An advantage of moment summation of aftershocks as opposed to the more usual counting earthquake numbers, is that as in Fig. 4 early in an aftershock sequence many small events may be missing from the catalog (Kagan, 2004). This under-count of small earthquakes gives an impression of aftershock rate saturation or rate decay when approaching the mainshock rupture end (i.e., going backwards in time towards the mainshock). In contrast, most of the moment in a sequence is carried by the strongest aftershocks, hence the bias in moment summation is less significant. However,

summation of seismic moments carries a significant price – random fluctuations of the sum are very large (Zaliapin *et al.*, 2005), hence more summands yield more reliable results.

Assuming that the aftershock size distribution follows the Gutenberg-Richter relation (Kagan, 2004), we can calculate the moment rate which is due to missing weak aftershocks and thus compensate for an incomplete catalog record. The part of the total seismic moment M_s in an aftershock time interval, which is missing due to incompleteness of the small earthquake record, can be obtained by modifying equation 21 in Kagan (2002).

$$F(M_s) \;=\; \left[\frac{M_a}{M_{xp}}\right]^{1-\beta}, \qquad (5)$$

where β is the parameter of earthquake size distribution ($\beta = 2b/3$), b is the b-value of the magnitude-frequency relation, M_a is the lower moment threshold for the aftershock sequence, and M_{xp} is the maximum moment. The threshold M_a depends on time according to (6). If $M_a = M_{xp}$, all moment is missing, whereas for $M_a \to 0$, the moment sum is complete.

For aftershock sequences we assume $\beta = 2/3$ (Kagan, 2002) and take the maximum moment (M_{xp}) to be the moment of the mainshock: if an earthquake stronger than the mainshock occurs during aftershock sequence, then the former mainshock would be re-classified as a foreshock. As alternative possibilities, we equate M_{xp} to the moment of the largest aftershock in a time interval or to the largest aftershock in the sequence.

Helmstetter *et al.* (2005) found the following approximate relation between the magnitude completeness threshold $m_a(t,m)$ at time t (in days) after a mainshock of magnitude m

$$m_a(t,m) \;=\; m - 4.5 - 0.75\log_{10}(t). \qquad (6)$$

For several recent (1980-2004) southern California mainshocks (see Fig. 4 as an example), the magnitude completeness threshold has been as high as 4.5 shortly after the mainshock, dropping only to about 2 later in the sequence. The equation is plotted in Fig. 4. We use the above two equations to correct aftershock moment release curves for under-reporting small events.

After calculating the moment threshold (6), and using (3), we estimate the multiplicative correction coefficient

$$[1 - F(M_s)]^{-1}\,. \qquad (7)$$

Calculating the correction term (7) for different mainshocks and various choice of M_{xp} (see above), we found out that, as one should expect from expression (6), the correction is largest for smallest time intervals. Even for these intervals the correction is less than 50%. In Fig. 5 as well as in all the calculations below we take as the maximum moment M_{xp} in (7) the value of the largest aftershock in each of time intervals. Only for time intervals closest to the mainshock rupture end, is the difference between non-corrected and corrected values observable. In the second time interval, the largest aftershock was smaller than the assumed threshold value (6), thus no correction coefficient is calculated.

Fig. 6 shows scaled moment release rates for three California earthquakes and their aftershocks as well as averages of both sets. In averaging datasets here and below, we divide the sum either by the number of curves, or by the number of non-zero entries in a dataset. The reason for the latter version is that source-time functions for some earthquakes were not defined at the same time intervals. Here the difference between two methods of averaging is quite minor.

To average source time functions (s.t.f.) together, it is necessary to normalize for the effect of their varying seismic moments. Houston *et al.* (1998) and Houston (2001) scaled s.t.f.'s to a common moment of 10^{19} Nm as follows. Scaled moment rate $\dot{M}_{sc}$ and scaled time t_{sc} are given by

$$\dot{M}_{sc}(t_{sc}) = \dot{M}(t_{sc}) \times \left(10^{19}/M_m\right)^{2/3} \quad \text{Nm/s}, \qquad (8)$$

and

$$t_{sc} = t \times \left(10^{19}/M_m\right)^{1/3}, \qquad (9)$$

where M_m is the moment of a mainshock, $\dot{M}(t)$ and t are unscaled seismic moment rate (i.e., the original s.t.f.) and unscaled time respectively. These transformations are equivalent to normalizing the source-time function to $m = 6.67$ earthquake. The variables τ_{pk}, $\dot{M}_{pk}$, t, and c in the formula for moment rate decay with time (4) can be scaled similarly.

As in Fig. 5 the extrapolation of aftershock moment release rates according to Omori's law is approximately 1.5 orders of magnitude below the maximum of the scaled source-time function at about 5 scaled seconds. This would mean $k \approx 1/30$ in (4).

The seismic moment scaling with the 2/3 exponent as in (8) and averaging the obtained quantities correspond to summation of earthquake rupture areas

$$S \;\propto\; M^{2/3}. \qquad (10)$$

When we sum aftershock numbers in the standard application of Omori's law, small events dominate the sum. In a sum of seismic moments of events with a Gutenberg-Richter distribution with $\beta = 2/3$, the largest earthquake on average carries 1/3 of the total moment (Zaliapin *et al.*, 2005). For $\beta = 2/3$, the average of earthquake rupture areas balances the influence of large and small earthquakes (Rundle, 1989).

3.2. Global shallow earthquakes

To make a more general comparison between moment release rates during mainshocks and those during aftershock sequences, we compare average scaled source time functions for several sets of global large shallow earthquakes with scaled aftershock sequences of six California mainshocks. Houston (2001) studied 255 source time functions determined by inversions of teleseismic body waves by Tanioka & Ruff (1997) and colleagues at the University of Michigan. Figure 7 shows the average of the scaled time functions of 143 events with depths between 5 and 40 km ranging in size from m 6.2 to 8.3. In the scaling and averaging procedure, these time functions were truncated (i.e., assumed to be zero) after the duration picked as the end of rupture by Tanioka and Ruff and colleagues (Houston, 2001). After its maximum, the average decreases exponentially with time (dashed and solid lines, Fig. 7).

Since picking the end of rupture from the inversion result is a subjective procedure and ignores possible moment release during an interval of interest, we also constructed the averages of three subsets of events for which the inversion included a sufficient interval after the apparent end of mainshock rupture. Specifically, we selected those events which had the inversion result available for at least 25, 30 or 40 sec, respectively, of scaled time. In averaging these events, the moment release rate was not truncated at the assumed end of rupture. These subsets contain 23, 15 and 8 events, respectively, so their averages are inherently more variable. Whereas the average of the truncated scaled time functions (dashed and solid lines) follows an exponential falloff with time, the average of the non-truncated scaled time functions

(dotted and thin solid lines) follows a power-law falloff similar to Omori's law (Fig. 7).

Most likely both selection criteria are biased. In the first case the possible continuation of moment release after a minimum in activity is ignored; in the second case, the selected source-time functions tend to have longer than average duration because a significant moment release was observed in later stages of earthquake rupture. Ideally, to study moment release rates in the first few tens to hundreds of seconds following mainshocks, one would average many source time functions based on the inversions of waveforms that continue for a sufficient length of time after the apparent end of rupture. A large consistent set of such time functions is not presently available.

Fig. 8 compares average source-time function with scaled and corrected aftershock moment rates for six California earthquakes, similar to Fig. 6. These sequences are for the 1952 Kern County, the 1992 Joshua Tree, 1992 Landers, 1992 Big Bear, the 1994 Northridge, and 1999 Hector Mine earthquakes. Although the Big Bear earthquake was an aftershock of the Landers event, it has an extensive aftershock sequence of its own which has all the properties of a regular mainshock event. We calculated the ratio of total moment release in the aftershock sequences to the seismic moment of the mainshock. The percentages are 6.3%, 12%, 5.8%, 19%, 12%, and 2.8%, respectively. After correction for missing small aftershocks, they are 6.8%, 13%, 6.5%, 21%, 14%, and 3.3%, respectively. As explained earlier, the correction is in general small; only for those time intervals closest to the end of mainshock rupture, does it reach several tens of percent.

In Fig. 9 scaled moment release rates of the aftershock sequences are averaged. The average behavior is similar to that of Fig. 6: an extrapolation of the average aftershock moment rate according to Omori's law (assuming $c = 0$) is about 1.5 orders of magnitude below the maximum of the source-time function, i.e., $k \approx 1/30$ in (4).

Figs. 6 and 8 compare the seismic moment release of mainshocks and aftershocks. Such a comparison can be made only retrospectively, i.e., only after an aftershock sequence has ended, do we know that the first (main) event is not followed by even stronger shock. For example, the M6.1 1992 Joshua Tree, California earthquake which occurred on April 23, 1992, was followed 66 days later by the M7.3 June 28 Landers event. Another example is the earthquake sequence in New Ireland region, where on November 16-17, 2000, four earthquakes with surface-wave magnitude from 7.2 to 8.2 occurred. Hence, were we to predict its aftershock decay, the forecast would be significantly wrong (Kagan, 2004). Therefore, our results relate to *typical* aftershock sequences, i.e., such that no earthquake comparable or stronger than the mainshock occurs in the sequence. Similarly the ratio of mainshock moment to the total moment of aftershock sequence, discussed above, would substantially change if unusual earthquake clusters are considered.

4. Discussion

4.1. Comparison of source-time functions and aftershock moment release

We compared average source-time functions for large shallow earthquakes with the ensuing moment release of immediate aftershocks. The global and California earthquakes are plotted against the average aftershock curves of California events. In both of these cases the pattern is similar: aftershock moment release follows Omori's law with the p-value (i.e., exponent in Eq. 2) close to 1.0. If the average curve is extrapolated toward the earthquake origin time, its continuation is about 30 times below the maximum of the average source-time function at the scaled time of about 5 s, which corresponds to the maximum release of seismic moment for a $m = 6.7$ earthquake. Taking into account the size of the focal zone for such an earthquake (about 20 km) and the average rupture velocity (2-3 km/s), this time seems to be reasonable for a bi-lateral rupture. The value of k in (4) found here, $k \approx 1/30$, is consistent with the rule of thumb known as Båth's law (Console *et al.*, 2003) which holds that the magnitude of the largest aftershock in a sequence is roughly 1-1.2 units smaller than that of the mainshock.

Around scaled time interval 20-60 s there is no moment release activity either in the source-time functions or in aftershock curves. This gap is most likely caused by the mainshock coda, which hinders aftershock detection. If this conjecture is true, one can extrapolate aftershock curves right to the end of earthquake rupture. Because of the coda wave interference we cannot extend the aftershock moment rate right to the end of mainshock rupture, but it seems likely that the transition of mainshock rupture into the aftershock process is smooth.

What might explain the difference between the rate of seismic moment release during mainshock rupture and that extrapolated from the aftershock moment release via Omori's law? The earthquake rupture process is most likely controlled by dynamic stresses: a rupture front is concentrated in a pulse (Heaton, 1990) with a strong stress wave initiating rupture. In contrast, the aftershock process is essentially static in that dynamic waves generated by an aftershock have almost always left the mainshock focal region before occurrence of a subsequent aftershock. According to various evaluations (Antonioli *et al.*, 2002; 2004; Gomberg *et al.*, 2003; Kilb *et al.*, 2002) the amplitude of the dynamic stress wave is at least an order of magnitude stronger than the amplitude of the incremental static stress. If the number and total moment release of both aftershocks and the rupture events comprising the mainshocks are proportional to the stress increase, we would expect the source-time function to be higher than the appropriately scaled aftershock moment release rate. This may explain the difference in moment release rates for mainshocks and aftershock sequences.

Moreover, it is likely that the temporal and spatial properties of earthquake rupture differ significantly from those of an aftershock distribution. Spatially, aftershock patterns are not different from the general earthquake distribution; they seem to be fractally distributed with a correlation dimension close to 2 (Robertson *et al.*, 1995; Guo & Ogata, 1997). Although it seems likely that the aftershock cloud is slowly expanding with time after a strong earthquake, there is no obvious strong order in the space-time distribution of aftershocks. Earthquake rupture, on the contrary, has clear pattern associated with rupture driven by propagating seismic waves (e.g., Heaton, 1990). Although the propagation of rupture has many complex features, like temporary stops, change of slip direction, jumping from one fault segment to another (see more discussion in Kagan, 2004), in general the spatio-temporal evolution of rupture exhibits significantly more orderly behavior than that of an aftershock sequence. Unfortunately, presently there are insufficient amount of data in earthquake source inversions for statistical analysis of the rupture propagation complexity.

4.2. Reasons for non-zero c-value

Our investigations and analysis of Omori's law (1) seem to suggest that the parameter c is either close to zero or should be a small negative value. What are the reasons for positive values of c which have been reported by many researchers? Kagan (2004) summarizes some of the possible causes: 1) the overlapping of seismic records in the wake of a strong earthquake; 2) workforce constraint which prevents detailed interpretation of complex seismograms during

the beginning of an aftershock sequence; 3) absence or malfunction of seismic stations close to the source zone; 4) the extended spatio-temporal character of earthquake rupture zone implying failure of the point model of the earthquake source; 5) temporary deployment of seismic stations introduces a new factor in identification and counting of aftershocks, a factor which is difficult to quantitatively evaluate. In sum, empirically-determined positive values for c arise largely from fitting the functional form of the Omori law to systematically under-counted numbers of aftershocks at early times following a mainshock.

What is the time interval between the end of mainshock rupture and the beginning of the aftershock sequence? Our results shown in Figs. 6, 8, and 9 indicate that the interval is small, no longer than 20-60 sec of scaled time, perhaps it is effectively equal to zero. The end of mainshock rupture is defined by a relatively low level of moment release. If the release is still high, this is considered as a continuation of the earthquake rupture process. Hence, the low-level interval is assumed in the definition of rupture duration during the retrospective interpretation of seismic records. As we suggested, an objective way to study the late part of the mainshock moment release and the beginning aftershock sequence, would be to process all the seismic records to a pre-arranged scaled time interval.

How then can one self-consistently identify an individual earthquake event? One criterion is to define the end of an individual event by rare (low probability) time interval without strong aftershocks. Another is to look at dynamic stress waves at certain amplitude (or other characteristic property) in a source zone of an earthquake. An earthquake is considered to end when there all such waves ceased. Both of these definitions depend on some quantitative criterion, and that most likely, the number and properties of such identified individual events would depend strongly on the value adopted.

5. Conclusions

Moment release rates during mainshocks (i.e., source time functions) are compared with moment release rates during aftershock sequences.

From minutes to months following a mainshock, the moment release rate of the aftershock sequence follows a power-law decay similar to the familiar Omori law for aftershock frequency. We note inconsistencies in the standard Omori formula, and propose that the positive values for c found empirically by many studies are mainly due to the under-reporting of small aftershocks. We used a time-dependent magnitude threshold to approximately estimate corrections to the aftershock moment rate for this effect.

We made several comparisons of individual California mainshocks and global averages of shallow mainshocks with individual aftershock sequences and with an average California aftershock sequence. Before averaging, the mainshock time functions and the aftershock moment release rates were scaled to normalize for the effect of varying mainshock seismic moments.

In all the comparisons, the extrapolation of the aftershock moment rates back in time following Omori's law yields a rate about 30 times smaller than the maximum moment rate of the mainshock. This disparity reflects the difference between the process of mainshock rupture, which is highly organized in space and time by dynamically propagating stress waves, and the process of aftershock nucleation, which spans a much greater temporal extent.

Acknowledgments. We appreciate partial support from the National Science Foundation through grants EAR 00-01128, EAR 04-09890, DMS-0306526, from CalTrans grant 59A0363, and from the Southern California Earthquake Center (SCEC). SCEC is funded by NSF Cooperative Agreement EAR-0106924 and USGS Cooperative Agreement 02HQAG0008. The authors thank J. Vidale and D. D. Jackson of UCLA for very useful discussions. Publication 0000, SCEC.

References

Agnew, D. C., 2005. Earthquakes: Future shock in California, *Nature*, **435**, 284-285, doi: 10.1038/435284a.

Antonioli, A., M. E. Belardinelli & M. Cocco, 2004. Modelling dynamic stress changes caused by an extended rupture in an elastic stratified half-space, *Geophys. J. Int.*, **157**(1), 229-244.

Antonioli, A., M. Cocco, S. Das & C. Henry, 2002. Dynamic stress triggering during the great 25 March 1998 Antarctic Plate earthquake, *Bull. Seismol. Soc. Amer.*, **92**(3), 896-903.

Console, R., A. M. Lombardi, M. Murru & D. Rhoades, 2003. Båth's law and the self-similarity of earthquakes, *J. Geophys. Res.*, **108**(B2), 2128.

Chen, Y.-L., C. G. Sammis & T.-L. Teng, 2004. A high frequency view of 1999 Chi-Chi, Taiwan, source rupture and fault mechanics, *Eos Trans. AGU*, **85**(47), Fall Meet. Suppl., Abstract S33C-07.

Chen, Y.-L., C. G. Sammis & T.-L. Teng, 2005. A high frequency view of 1999 Chi-Chi, Taiwan, source rupture and fault mechanics, *Bull. Seismol. Soc. Amer.*, submitted.

Dreger, D. S., 1994. Investigation of the rupture process of the 28 June 1992 Landers earthquake utilizing TERRASCOPE, *Bull. Seismol. Soc. Amer.*, **84**(3), 713-724.

Gerstenberger, M. C., S. Wiemer, L. M. Jones & P. A. Reasenberg, 2005. Real-time forecasts of tomorrow's earthquakes in California, *Nature*, **435**, 328-331, doi: 10.1038/nature03622.

Gomberg, J., P. Bodin & P. A. Reasenberg, 2003. Observing earthquakes triggered in the near field by dynamic deformations, *Bull. Seismol. Soc. Amer.*, **93**, 118-138.

Guo, Z. & Y. Ogata, 1997. Statistical relations between the parameters of aftershocks in time, space, and magnitude, *J. Geophys. Res.*, **102**, 2857-73.

Hanks, T.C., 1992. Small earthquakes, tectonic forces, *Science*, **256**, 1430-1432.

Heaton, T. H., 1990. Evidence for and implications of self-healing pulses of slip in earthquake rupture, *Phys. Earth Planet. Inter.*, **64**, 1-20.

Helmstetter, A., Y. Y. Kagan & D. D. Jackson, 2005. Comparison of short-term and long-term earthquake forecast models for Southern California, *Bull. Seismol. Soc. Amer.*, submitted http://scec.ess.ucla.edu/~ykagan/agnes_index.html .

Houston, H., 2001. Influence of depth, focal mechanism, and tectonic setting on the shape and duration of earthquake source time functions, *J. Geophys. Res.*, **106**, 11,137-11,150.

Houston, H., H. M. Benz & J. E. Vidale, 1998. Time functions of deep earthquakes from broadband and short-period stacks, *J. Geophys. Res.*, **103**(B12), 29,895-29,913.

Hutton, L. K. & L. M. Jones, 1993. Local magnitudes and apparent variations in seismicity rates in Southern California, *Bull. Seismol. Soc. Am.*, **83**, 313-329.

Ji, C., D. J. Wald & D. V. Helmberger, 2002. Source description of the 1999 Hector Mine, California, earthquake, part I: Wavelet domain inversion theory and resolution analysis, *Bull. Seismol. Soc. Amer.*, **92**(4), 1192-1207.

Kagan, Y. Y., 2002. Seismic moment distribution revisited: II. Moment conservation principle, *Geophys. J. Int.*, **149**, 731-754.

Kagan, Y. Y., 2004. Short-term properties of earthquake catalogs and models of earthquake source, *Bull. Seismol. Soc. Amer.*, **94**(4), 1207-1228.

Kanamori, H. & E. E. Brodsky, 2004. The physics of earthquakes, *Rep. Prog. Phys.*, **67**, 1429-1496, doi:10.1088/0034-4885/67/8/R03.

Kilb, D., J. Gomberg & P. Bodin, 2002. Aftershock triggering by complete Coulomb stress changes, *J. Geophys. Res.*, **107**(B4), 2060.

Ogata, Y., 1983. Estimation of the parameters in the modified Omori formula for aftershock frequencies by the maximum likelihood procedure, *Journal of Physics of the Earth*, **31**, 115-124.

Omori, F., 1894. On the after-shocks of earthquakes, *J. College Sci., Imp. Univ. Tokyo*, **7**, 111-200, (with Plates IV-XIX).

Peng, Z. & Vidale, J. E., 2004. Early aftershock decay rate of the M6 Parkfield earthquake, *Eos Trans. AGU*, **85**(47), Fall Meet. Suppl., Abstract S51C-0170X.

Reasenberg, P. A. & L. M. Jones, 1989. Earthquake hazard after a mainshock in California, *Science*, **243**, 1173-1176.

Reasenberg, P. A. & L. M. Jones, 1994. Earthquake aftershocks: Update, *Science*, **265**, 1251-1252.

Robertson, M. C., C. G. Sammis, M. Sahimi & A. J. Martin, 1995. Fractal analysis of three-dimensional spatial distributions of earthquakes with a percolation interpretation, *J. Geophys. Res.*, **100**, 609-20.

Rundle, J. B., 1989. Derivation of the complete Gutenberg-Richter magnitude-frequency relation using the principle of scale invariance, *J. Geophys. Res.*, **94**, 12,337-12,342.

Rundle, J. B., D. L. Turcotte, R. Shcherbakov, W. Klein & C. Sammis, 2003. Statistical physics approach to understanding the multiscale dynamics of earthquake fault systems, *Rev. Geophys.*, **41**(4), 1019.

Shcherbakov, R., D. L. Turcotte & J. B. Rundle, 2004. A generalized Omori's law for earthquake aftershock decay, *Geophys. Res. Lett.*, **31**(11), L11613, 10.1029/2004GL019808.

Tanioka, Y. & L. Ruff, 1997. Source time functions, *Seismol. Res. Lett.*, **68**(3), 386-397.

Thio, H. K. & H. Kanamori, 1996. Source complexity of the 1994 Northridge earthquake and its relation to aftershock mechanisms, *Bull. Seismol. Soc. Amer.*, **86**, S84-S92.

Utsu, T., 1961. A statistical study on the occurrence of aftershocks, *Geoph. Magazine*, **30**, 521-605.

Utsu, T., Y. Ogata & R. S. Matsu'ura, 1995. The centenary of the Omori formula for a decay law of aftershock activity, *J. Phys. Earth*, **43**, 1-33.

Vidale, J. E., E. S. Cochran, H. Kanamori & R. W. Clayton, 2003. After the lightning and before the thunder; non-Omori behavior of early aftershocks? *Eos Trans. AGU* **84**(46), Fall Meet. Suppl., Abstract S31A-08.

Vidale, J. E., Z. Peng & M. Ishii, 2004. Anomalous aftershock decay rates in the first hundred seconds revealed from the Hinet borehole data, *Eos Trans. AGU*, **85**(47), Fall Meet. Suppl., Abstract S23C-07.

Wiemer, S., M. Gerstenberger & E. Hauksson, 2002. Properties of the aftershock sequence of the 1999 M_w 7.1 Hector Mine earthquake: Implications for aftershock hazard, *Bull. Seismol. Soc. Amer.*, **92**, 1227-1240.

Wiemer, S. & K. Katsumata, 1999. Spatial variability of seismicity parameters in aftershock zones, *J. Geophys. Res.*, **104**, 13135-13151.

Zaliapin, I. V., Y. Y. Kagan & F. Schoenberg, 2005. Approximating the distribution of Pareto sums, *Pure Appl. Geoph.*, **162**(6-7), 1187-1228.

Yan Y. Kagan, Department of Earth and Space Sciences, University of California, Los Angeles, California, 90095-1567, USA; (e-mail: ykagan@ucla.edu)

Heidi Houston, Department of Earth and Space Sciences, University of California, Los Angeles, California, 90095-1567, USA; (e-mail: hhouston@ess.ucla.edu)

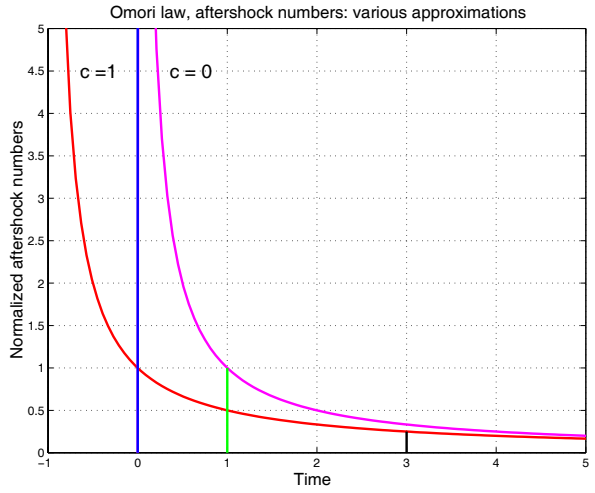

Figure 1. A positive $c > 0$ in Omori's law means that the singularity in aftershock rate occurs at negative time ($t < 0$), i.e., before the mainshock. We show Omori laws with $c = 1$ and $c = 0$ here in linear scale and below in log-log scale (Fig. 2). Positive c would fit a relative lack of early aftershocks (either real or apparent), but trends toward a singularity before the mainshock initiation. We propose that the positive empirical value for c is mostly due to the under-reporting of small aftershocks immediately following a mainshock (Kagan, 2004).

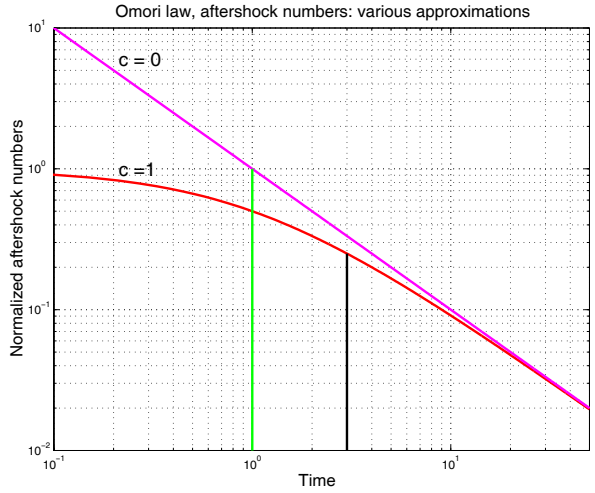

Figure 2. Same as Fig. 1 but in log-log scale.

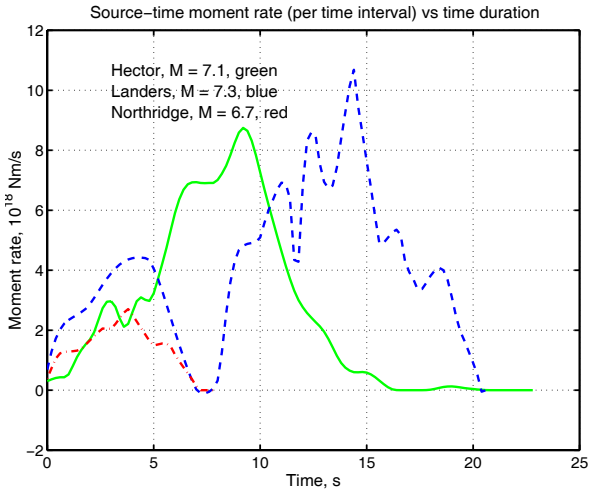

Figure 3. Seismic moment source-time functions for three California earthquakes: 1992 $M7.3$ Landers (dashed line), 1994 $M6.7$ Northridge (dash-dotted line), and 1999 $M7.1$ Hector Mine (solid line).

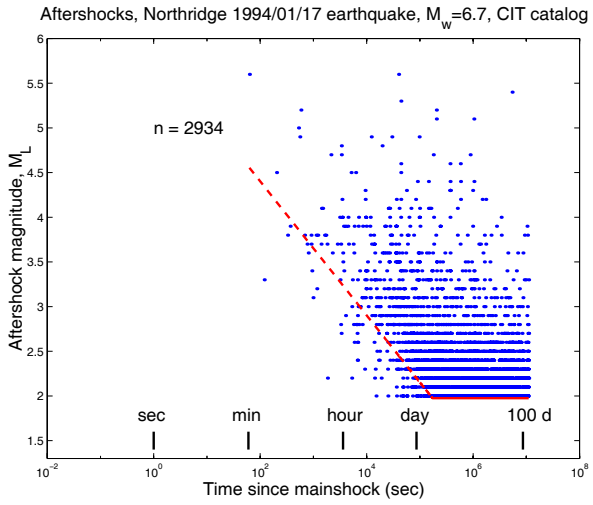

Figure 4. Time-magnitude distribution of 1994/01/17 $M = 6.7$ Northridge, California aftershocks. The CalTech earthquake catalog is used. Events in the 128 days following the mainshock and between latitude 34.0°N and 34.5°N and longitude 118.35°W and 118.80°W were selected. The dashed line shows an estimate of the completeness threshold (Equation 7), which can be used to correct aftershock frequency and moment release rate for missing aftershocks.

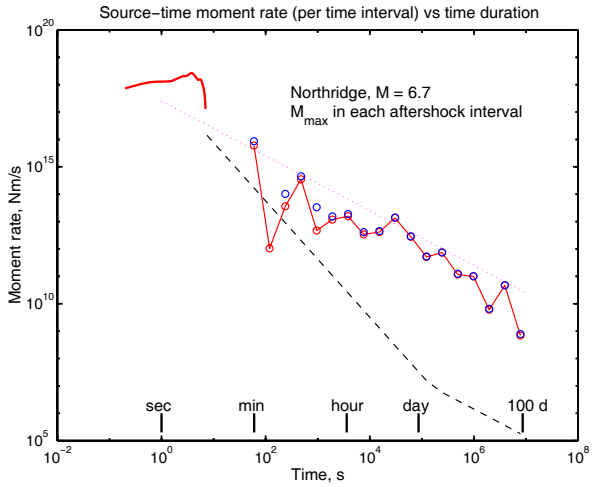

Figure 5. Source-time function for 1994 $M6.7$ Northridge, California earthquake compared to moment release (red circles) of its immediate aftershocks, averaged over logarithmic time intervals. Blue circles show aftershock moment release corrected for under-reported small aftershocks (7), using the aftershock moment threshold (black dashed line) divided by the duration of the corresponding time interval to yield quantities comparable to the moment rate. The dotted line shows a power-law approximation for aftershock moment release rates, analogous to Omori's law (1).

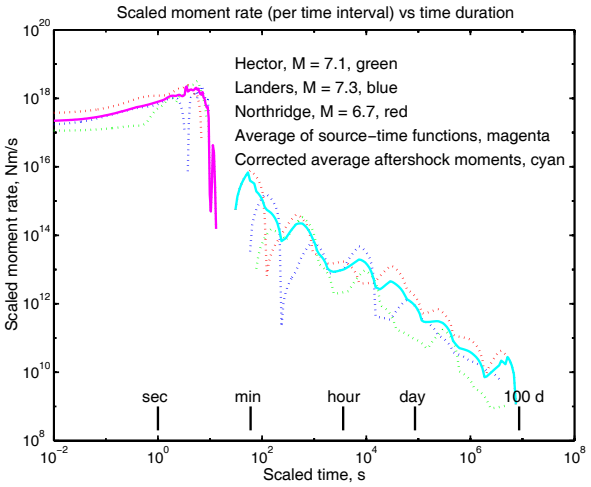

Figure 6. Scaled source-time functions for three California earthquakes: 1992 $M7.3$ Landers (dashed line), 1994 $M6.7$ Northridge (dash-dotted line), and 1999 $M7.1$ Hector Mine (solid line) and moment release of their immediate aftershocks, corrected for missing small aftershocks (7) and averaged over logarithmic time intervals. Source time functions and aftershock moment release rates were normalized to account for the effect of varying mainshock moments, allowing the averaging of data for mainshocks of different size. Here we scale all mainshocks and aftershock sequences to a magnitude 6.67 event.

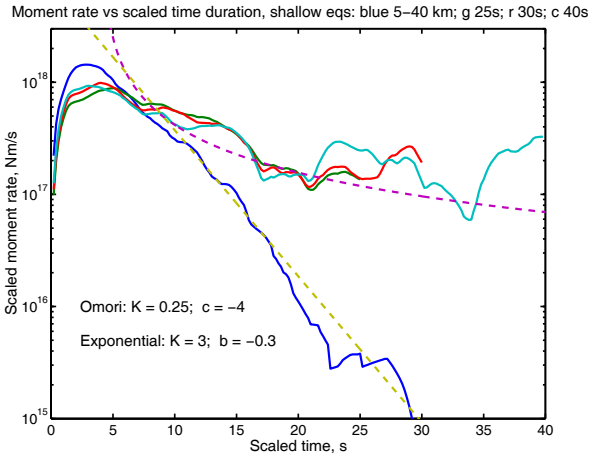

Figure 7. Average scaled seismic moment source-time functions for 143 shallow (5-40 km) global earthquakes, and their approximation by an exponential function (yellow) and a power-law (Omori's) distribution. For the latter approximation we use $c = -4$ s which is close to the rupture time of $m = 6.67$ earthquake. The blue curve shows the average of scaled time functions truncated at the inferred end of rupture. Green, red, and cyan curves show averages of subsets of source-time functions comprising those non-truncated time functions for which the s.t.f inversion result was available for at least 25, 30, and 40 scaled seconds (i.e., including a sufficient interval after the apparent end of mainshock rupture). For the non-truncated time functions, moment release at the end of mainshock rupture seems to decay as $1/t$ similar to Omori's law.

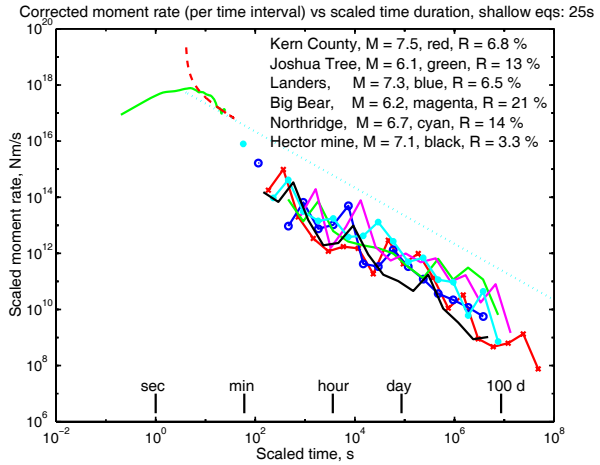

Figure 8. Average scaled source-time function for shallow global earthquakes compared to scaled aftershock moment release rates for six California aftershock sequences. The average includes only events with inversion results available for at least 25 s of scaled time. Both types of moment rates were scaled to a magnitude 6.67 event. Two Omori law approximations to the source time functions are shown with $c = -4$ s (dashed magenta line), and with $c = 0$ s (dotted blue line). The California aftershock sequences were corrected for missing small aftershocks (following Eq. 7). The coefficient R in the figure is the percent of total seismic moment released by immediate aftershocks compared to the mainshock scalar moment. The activity level in the aftershock sequences extrapolates to about 30 times less than the peak rate in the average scaled global time function.

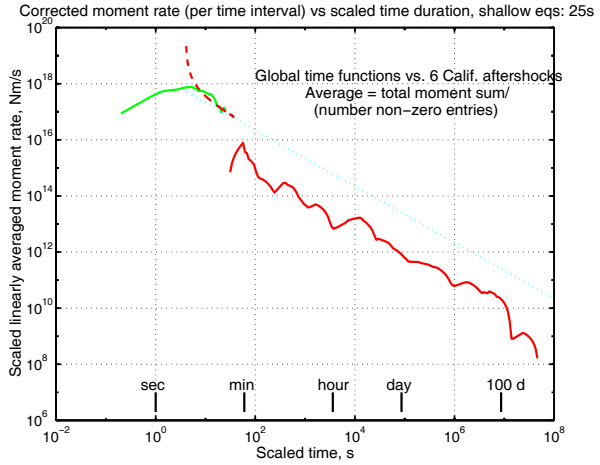

Figure 9. Average scaled source-time function for global shallow earthquakes with non-truncated time functions (green line) compared to the corrected scaled average for six California aftershock sequences (red line). Approximations of average time function by power-law (Omori) distributions (dashed and dotted lines) are also shown. As before, two Omori law approximations are given with $c = -4$ s, and with $c = 0$ s. The average aftershock rates fall about 8 orders of magnitude over about 200 days. Extrapolating back in time according to Omori's law yields a level of aftershock activity about 1.5 orders of magnitude less than the maximum mainshock moment rate.